New variable transformations for evaluating nearly singular integrals in 3D boundary element method

Guizhong Xie, Fenglin Zhou, Jianming Zhang*, Xingshuai Zheng, Cheng Huang

State Key Laboratory of Advanced Design and Manufacturing for Vehicle Body, College of Mechanical and Vehicle Engineering, Hunan University, Changsha 410082, China

Correspondence to: Jianming Zhang
College of Mechanical and Vehicle Engineering, Hunan University, Changsha 410082, China
Telephone: +86-731-88823061
E-mail: zhangjm@hnu.edu.cn

ABSTRACT

This work presents new variable transformations for accurate evaluation of the nearly singular integrals arising in the 3D boundary element method (BEM). The proposed method is an extension of the variable transformation method in Ref. [4] for 2D BEM to 3D BEM. In this paper, first a new system denoted as (α,β) is introduced compared with the polar coordinate system. So the original transformations in Ref. [4] can be developed to 3D in (α,β) or polar coordinate system. Then, the new transformation is performed by four steps in case the source point coincides with the projection point or five steps otherwise. For each step, a new transformation is proposed based on the approximate distance function, so that all steps can finally be unified into a uniform formation. To perform integration on irregular elements, an adaptive integration scheme combined with the transformations is applied. Numerical examples compared with other methods are presented. The results demonstrate that our method is accurate and effective.

KEYWORDS: nearly singular integrals, numerical integration, boundary element method, variable transformations.

1. Introduction

Near singularities are involved in many boundary element method (BEM) analyses of engineering problems, such as problems on thin shell-like structures [1-3], the crack problems [5], the contact problems [6], as well as the sensitivity problems [7]. Accurate and efficient evaluation of nearly singular integrals with various kernel functions of the type $O(1/r^{\chi})$ is crucial for successful implementation of the boundary type numerical methods based on boundary integral equations (BIEs), such as the boundary element method (BEM), the boundary face method (BFM) [8-13]. A near singularity arises when a source point is close to but not on the integration elements. Although these integrals are really regular in nature, they can't be evaluated accurately by the standard Gaussian quadrature. This is the so-called boundary layer effect in BEM and BFM. The boundary layer effect comes from the properties of fundamental solutions and their derivatives. The denominator *r*, the distance between the source and the field point, is close to zero but not zero. The difficulty encountered in the numerical evaluation mainly results from the fact that the integrands of nearly singular integrals vary drastically with the distance.

Effective computation of nearly singular integrals has received intensive attention in recent years. Various numerical techniques have been developed to remove the near singularities, such as rigid body displacement solutions [14], global regularization [15-18], semi-analytical or analytical integral formulas [19, 20], the sinh transformation [21-23], polynomial transformation [24], adaptive subdivision method [8, 9, 25, 26], distance transformation technique [11, 27-30], the $L_1^{-1/5}$ transformation [31] , the PART method [31-33] and the variable transformations [4]. Most of them benefit from the strategies for computing singular integrals. Among these techniques, variable transformations technique seems to be a more promising method for dealing with different orders of nearly singular integrals. However, the transformations are only limited to 2D boundary element. In this paper, we develop the variable transformations technique to evaluate the nearly singular integrals on parametric

surface used in BFM [8-13]. In our method, a new local coordinate system [8, 11] described by (α,β) is introduced. This system is very similar to the polar system, but its implementation is simpler as the polar system and also performs efficiently. So, the transformations in Ref. [4] can be extended to 3D in (α,β) or polar coordinates. We first take four steps to analyze the transformation when the distance between the source point and the projection point equals zero, and five steps otherwise. In each step, the mathematical derivation is presented in detail. Then these steps are unified into a uniform formation, in which the near weak and strong singularity can be removed. To perform integration on irregular elements, the element subdivision technique is employed in combination with our method. Although the element subdivision technique is used, the computational cost is reduced dramatically compared with the conventional element subdivision techniques [8, 9, 25, 26]. Our method has been successfully applied in the evaluation of nearly singular integrals on planar elements and curved surface elements. Numerical examples are presented for different cases regarding positions of the projection point and values of the minimum distance. Results demonstrate that our method is accurate and effective.

This paper is organized as follows. The general form of nearly singular integrals is described in Section 2. Section 3 briefly reviews the distance function in polar coordinate system. In Section 4, the distance function is constructed in (α,β) coordinate system with new form. In Section 5, the transformations for nearly singular integrals are presented in detail. In section 6, element subdivision is introduced. Numerical examples are given in Section 7. The paper ends with conclusions in Section 8.

2. General descriptions

In this paper, we will deal with the computation of integrals of the following form

$$I=\int_S \frac{f(\mathbf{x},\mathbf{y})}{r^l}dS,\quad l=1,2,3 \qquad r=\|\mathbf{x}-\mathbf{y}\|_2 \tag{1}$$

Where f is a smooth function, $\mathbf{x}$ and $\mathbf{y}$ represent the field point and the source point in BEM, with components x_i and y_i, (i=1, 2, 3), respectively. S represents the boundary element. We assume that the source point is close to S, but not on it.

For simplicity, let us take the three-dimensional potential problems as an example. The two boundary integral equations are given by

$$c(\mathbf{y})u(\mathbf{y}) = \int_\Gamma q(\mathbf{x})u^*(\mathbf{x},\mathbf{y})d\Gamma(\mathbf{x}) - \int_\Gamma u(\mathbf{x})q^*(\mathbf{x},\mathbf{y})d\Gamma(\mathbf{x}) \tag{2}$$

$$c(\mathbf{y})u_k(\mathbf{y}) = \int_\Gamma q(\mathbf{x})u_k^*(\mathbf{x},\mathbf{y})d\Gamma(\mathbf{x}) - \int_\Gamma u(\mathbf{x})q_k^*(\mathbf{x},\mathbf{y})d\Gamma(\mathbf{x}) \tag{3}$$

where c is a coefficient depending on the smoothes of the boundary at the source point $\mathbf{y}$ [31]. $u^*(\mathbf{x},\mathbf{y})$ is the fundamental solution for 3D problem expressed as:

$$u^*(\mathbf{x},\mathbf{y}) = \frac{1}{4\pi}\frac{1}{r(\mathbf{x},\mathbf{y})},\quad q^*(\mathbf{x},\mathbf{y}) = -\frac{1}{4\pi}\frac{(\mathbf{r},\mathbf{n})}{r^3(\mathbf{x},\mathbf{y})} \tag{4}$$

$$u_k^*(\mathbf{x},\mathbf{y}) = \frac{\partial u^*(\mathbf{x},\mathbf{y})}{\partial x_k},\quad q_k^*(\mathbf{x},\mathbf{y}) = \frac{\partial q^*(\mathbf{x},\mathbf{y})}{\partial x_k} \tag{5}$$

Where $\mathbf{n}$ is the unit outward direction to the boundary Γ, with components n_i, (i=1, 2, 3). Eq. (2) and Eq. (3) are discretized on the boundary Γ by boundary elements $\Gamma_e (e = 1 \sim N)$ defined by interpolation functions. The integral kernels of Eq. (2) and (3) become nearly singular when the distance between the source point and integration element is very small compared to the size of integration element. And integrals in Eq. (2) and Eq. (3) become near singularity with different levels considering χ in Eq. (1), namely, u^* with near weak singularity, u_k^* and q^* with near strong singularity, and q_k^* with near hyper singularity. In this paper, we develop new variable transformations method for various boundary integrals with near singularities of different levels. The new method is detailed in following sections. For the sake of clarity and brevity, we take following integrals in a general form to discuss:

$$I = \int_S O(1/r^l)\phi dS \tag{6}$$

3. Review definition of the distance polar coordinate system

In this section, we will briefly review the distance function [11, 27-30].

As shown in Fig.1, employing the first-order Taylor expansion in the neighborhood of the projection point $\mathbf{x}^c$, we have

$$\begin{aligned} x_k - y_k &= x_k - x_k^c + x_k^c - y_k \\ &= \left.\frac{\partial x_k}{\partial t_1}\right|_{\substack{t_1=c_1 \\ t_2=c_2}} (t_1 - c_1) + \left.\frac{\partial x_k}{\partial t_2}\right|_{\substack{t_1=c_1 \\ t_2=c_2}} (t_2 - c_2) + r_0 n_k(c_1, c_2) + O(\rho^2) \\ &= \rho A_k(\theta) + r_0 n_k(c_1, c_2) + O(\rho^2) \end{aligned} \tag{7}$$

where (c_1, c_2) are the coordinates of the projection point in a local system (t_1, t_2), $\rho = \sqrt{(t_1 - c_1)^2 + (t_2 - c_2)^2}$ and $r_0 = \left\| \mathbf{x}^c - \mathbf{y} \right\|$ which is the minimum distance from the source point to the element in most cases. r_0 is equal to zero when $\mathbf{y}$ is located on the tangential plane through $\mathbf{x}^c$. n_k (k=1, 2, 3) represents the component of the unit outward direction to the surface boundary and

$$A_k(\theta) = \left.\frac{\partial x_k}{\partial t_1}\right|_{\substack{t_1=c_1 \\ t_2=c_2}} \cos\theta + \left.\frac{\partial x_k}{\partial t_2}\right|_{\substack{t_1=c_1 \\ t_2=c_2}} \sin\theta \tag{8}$$

So, we can get the distance function

$$r^2 = (x_k - y_k)(x_k - y_k) = A_k^2(\theta)\rho^2 + r_0^2 + O(\rho^3) \tag{9a}$$

$$r = \sqrt{A_k^2(\theta)\rho^2 + r_0^2 + O(\rho^3)} \tag{9b}$$

So, using Eq. (9a) and Eq. (9b), Eq. (1) can be written as

$$I = \int_\Gamma \frac{f(\mathbf{x}, \mathbf{y})}{r^l} d\Gamma = \sum_m \int_{\theta_m}^{\theta_{m+1}} \int_{\rho_1(\theta)}^{\rho_2(\theta)} \frac{g(\rho, \theta)}{(\rho^2 + \omega^2(\theta))^{l/2}} d\rho d\theta \tag{10}$$

where $\omega(\theta) = \dfrac{r_0}{A(\theta)}$, $A(\theta) = \sqrt{A_k(\theta) A_k(\theta)}$, and $g(\rho, \theta)$ is a smooth function.

4. Construct new definition of the distance function in (α, β) coordinate system

To construct the new distance function, firstly, a quadrilateral element in the local parameter (t_1, t_2) space which the projection point is located in the element is

considered. As shown in Fig. 2(*a*) and Fig. 2(*b*), the element is divided into four triangles in the parameter space. For each triangle, the following mapping [8, 11] is used

$$\begin{cases} t_1^a = c_1 + (t_1^1 - c_1)\alpha \\ t_2^a = c_2 + (t_2^1 - c_2)\alpha \end{cases} \tag{11}$$

$$\begin{cases} t_1^b = c_1 + (t_1^2 - c_1)\alpha \\ t_2^b = c_2 + (t_2^2 - c_2)\alpha \end{cases} \tag{12}$$

$$\begin{cases} t_1 = t_1^a + (t_1^b - t_1^a)\beta \\ t_2 = t_2^a + (t_2^b - t_2^a)\beta \end{cases} \quad \alpha, \beta \in [0,1] \tag{13}$$

Combining Eqs. (11)-(13), the expression, which is different to obtain the coordinates t_1 and t_2 compared with the polar coordinate system above, can be written as

$$\begin{cases} t_1 = c_1 + (t_1^1 - c_1)\alpha + (t_1^2 - t_1^1)\alpha\beta \\ t_2 = c_2 + (t_2^1 - c_2)\alpha + (t_2^2 - t_2^1)\alpha\beta \end{cases} \tag{14}$$

As shown in Fig. 2(*c*), the triangle is mapped onto a square [0, 1]×[0, 1] of unit side-length in (α, β) coordinate system using the transformation (14). Both α and β are constrained to interval [0, 1] in each triangle and there is no need to compute their spans. On the contrary, the spans for ρ and θ in the polar system should be evaluated. The Jacobian for the transformation from (t_1, t_2) system to (α, β) system is αS_Δ, and

$$S_\Delta = \left| t_1^1 t_2^2 + t_1^2 c_2 + c_1 t_2^1 - t_1^2 t_2^1 - c_1 t_2^2 - t_1^1 c_2 \right| \tag{15}$$

So, using Eqs. (11) - (14)

$$\begin{aligned} x_k - y_k &= x_k - x_k^c + x_k^c - y_k \\ &= \left.\frac{\partial x_k}{\partial t_1}\right|_{\substack{t_1=c_1 \\ t_2=c_2}} (t_1 - c_1) + \left.\frac{\partial x_k}{\partial t_2}\right|_{\substack{t_1=c_1 \\ t_2=c_2}} (t_1 - c_2) + r_0 n_k(c_1, c_2) + O(\alpha^2) \\ &= \alpha A_k(\beta) + r_0 n_k(c_1, c_2) + O(\alpha^2) \end{aligned} \tag{16}$$

in which

$$A_k(\beta)=\left.\frac{\partial x_k}{\partial t_1}\right|_{\substack{t_1=c_1\\ t_2=c_2}}\left[(t_1^1-t_1^0)+(t_1^2-t_1^1)\beta\right]+\left.\frac{\partial x_k}{\partial t_2}\right|_{\substack{t_1=c_1\\ t_2=c_2}}\left[(t_2^1-t_2^0)+(t_2^2-t_2^1)\beta\right] \quad (17)$$

Using Eqs. (10)-(17), we can easily obtain the distance function in a new form

$$r^2=(x_k-y_k)(x_k-y_k)=A_k^2(\theta)\alpha^2+r_0^2+O(\alpha^3) \quad (18a)$$

$$r=\sqrt{A_k^2(\theta)\alpha^2+r_0^2+O(\alpha^3)} \quad (18b)$$

So, using Eq. (18a) and Eq. (18b), Eq. (1) can be written as

$$I=\int_\Gamma \frac{f(\mathbf{x},\mathbf{y})}{r^l}d\Gamma=\sum_m\int_0^1\int_0^1\frac{g(\alpha,\beta)}{(\alpha^2+\lambda^2(\beta))^{l/2}}d\alpha d\beta \quad (19)$$

where $\lambda(\beta)=\dfrac{r_0}{A(\beta)}$, $A(\beta)=\sqrt{A_k(\beta)A_k(\beta)}$, and $g(\alpha,\beta)$ is a smooth function.

5. New variable transformations for nearly singular integrals

In this section, we construct efficient variable transformations to compute nearly singular integrals for different cases. Ref. [4] has given variable transformations to remove near singularity in 2D BEM, so it is time to extend these efficient transformations to 3D BEM. Those transformations are based on the idea that the integrands with the rapid variation are smoothed out and their integrals can be calculated precisely by the standard Gaussian quadrature. We will construct different transformations for the following three cases: (1) $r_0\neq 0$ and the projection point in the element as shown in Fig. 3(a); (2) $r_0=0$ and the projection point outside the element as shown in Fig. 3(b); (3) $r_0\neq 0$ and the projection point outside the element as shown in Fig. 3(c).

5.1 Case 1: $r_0\neq 0$ and the projection point in the element

Nearly singular integrals of this type arise when we computed the thin bodies. As shown in Fig. 4, when the source point is located on the bottom surface and the integration element is on the top surface, the projection point happens to lie in the integration element.

We will give different transformations considering the two coordinates, namely,

(α,β) and the polar coordinate system. In order to obtain a reasonable transformation for each case, the distance *r* is approximated by the Taylor expansion (9a) and (18a) without considering higher orders term as Eq. (9b) and Eq. (18b). However, in actual computation *r* is still the distance from the source point to the field point. We explain how to construct different transformations. The process consists of five steps and each step is described briefly below.

From Eq. (10) and Eq. (19), we can analyze that the near singularity is essentially related to the radial variable ρ and α. So we will construct a more robust and efficient transformation for the radial variable ρ and α.

First we only consider the radial variable integral which depicts near singularity in the Eqs. (10) and (19), as follows

$$I_1 = \int_{\rho_1(\theta)}^{\rho_2(\theta)} \frac{g(\rho,\theta)}{(\rho^2+\omega^2(\theta))^{l/2}} d\rho \tag{20a}$$

$$I_2 = \int_0^1 \frac{g(\alpha,\beta)}{(\alpha^2+\lambda^2(\beta))^{l/2}} d\alpha \tag{20b}$$

When the projection point is in the integration element, Eq. (20a) becomes the following form

$$I_1 = \int_0^{\rho_2(\theta)} \frac{g(\rho,\theta)}{(\rho^2+\omega^2(\theta))^{l/2}} d\rho \tag{20c}$$

Second we make a stretching transformation for Eq. (20c) and Eq. (20b) respectively

$$\rho = r_0\xi_1 \tag{21a}$$

$$\alpha = r_0\eta_1 \tag{21b}$$

Substituting Eq. (21a) into Eq. (20c), and Eq. (21b) into Eq. (20b), we have

$$I_1 = \int_0^{\frac{\rho_2(\theta)}{r_0}} \frac{r_0 g(\xi_1,\theta)}{(\xi_1^2+\omega^2(\theta))^{l/2}} d\xi_1 \tag{22a}$$

$$I_2 = \int_0^{\frac{1}{r_0}} \frac{r_0 g(\eta_1, \beta)}{(\eta_1^2 + \lambda^2(\beta))^{l/2}} d\eta_1 \tag{22b}$$

Then we make a translation transformation for Eqs. (22a) and (22b), respectively

$$\xi_2 = \xi_1 + 1 \tag{23a}$$

$$\eta_2 = \eta_1 + 1 \tag{23b}$$

This step is employed to adjust the lower limit of the integration variable for the afterward logarithmic transformation.

Substituting Eq. (23a) into Eq. (22a), Eq. (23b) into Eq. (22b), results in

$$I_1 = \int_1^{\frac{\rho_2(\theta)}{r_0}+1} \frac{r_0 g(\xi_2 - 1, \theta)}{((\xi_2 - 1)^2 + \omega^2(\theta))^{l/2}} d\xi_2 \tag{24a}$$

$$I_2 = \int_1^{\frac{1}{r_0}+1} \frac{r_0 g(\eta_2 - 1, \beta)}{((\eta_2 - 1)^2 + \lambda^2(\beta))^{l/2}} d\eta_2 \tag{24b}$$

In the four steps, we smooth out the rapid variations of the integrand by the following logarithmic transformation

$$\xi_3 = \log(\xi_2) \tag{25a}$$

$$\eta_3 = \log(\eta_2) \tag{25b}$$

Substituting Eqs. (25a)-(25b) into Eqs. (24a)-(24b), Eqs. (24a)-(24b) can be expressed as

$$I_1 = \int_0^{\log(\frac{\rho_2(\theta)}{r_0}+1)} \frac{r_0 g(e^{\xi_3} - 1, \theta) e^{\xi_3}}{((e^{\xi_3} - 1)^2 + \omega^2(\theta))^{l/2}} d\xi_3 \tag{26a}$$

$$I_2 = \int_0^{\log(\frac{1}{r_0})} \frac{r_0 g(e^{\eta_3} - 1, \beta) e^{\eta_3}}{((e^{\eta_3} - 1)^2 + \lambda^2(\beta))^{l/2}} de^{\eta_3} \tag{26b}$$

Using the good properties of the logarithmic function [27-30, 34, 35], it can easily be proved that the transformed integrand has much lower gradient.

Finally, adjusting the integration interval within [-1, 1] for performing the standard Gaussian quadrature directly, we propose the following transformation.

$$\xi_3 = k_1\xi_4 + k_1 \tag{27a}$$

where $k_1 = \frac{1}{2}\log(\frac{\rho_2(\theta)}{r_0} + 1)$

$$\eta_3 = k_2\eta_4 + k_2 \tag{27b}$$

where $k_2 = \frac{1}{2}\log(\frac{1}{r_0} + 1)$

Using the transformations (27a) and (27b), we have

$$I_1 = \int_{-1}^{1} \frac{k_1 r_0 g(e^{k_1\xi_4 + k_1}) - 1, \theta) e^{k_1\xi_4 + k_1}}{((e^{k_1\xi_4 + k_1} - 1)^2 + \omega^2(\theta))^{l/2}} d\xi_4 \tag{28a}$$

$$I_2 = \int_{-1}^{1} \frac{k_2 r_0 g(e^{k_2\eta_4 + k_2} - 1, \beta) e^{k_2\eta_4 + k_2}}{((e^{k_2\eta_4 + k_2} - 1)^2 + \lambda^2(\beta))^{l/2}} d\eta_4 \tag{28b}$$

We integrate all the transformations detailed above and can obtain the final transformation as

$$\rho = r_0(e^{k_1\xi + k_1} - 1) \tag{29a}$$

$$\alpha = r_0(e^{k_2\eta + k_2} - 1) \tag{29b}$$

It should be noted that we still use the exact *r* instead of the approximate *r* in Eq. (28a) and Eq. (28b), and that the nearly singular kernels are not changed into another forms. It should be also noted that the two variable transformations are similar to these in Refs. [34, 35]. However, the deductions in this paper are very different from those given in Refs. [34, 35]. We construct the transformations in a general way based on the approximate distance function derived from first-order Taylor expansion. Moreover, for the first time, the variable transformations are applied for evaluating

nearly singular integrals in 3D BEM.

5.2 Case 2: r_0=0 and the projection point outside the element

When r_0=0 and the projection point is outside the element, as shown in Fig. 3(b) and Fig. 5. When discontinuous elements or elements that sizes are quite different are adopted, nearly singular integrals of this type arise.

The process of constructing variable transformations is different from that described in Section 5.1. We also deduce corresponding transformations for this case and the process consisting of four steps is described briefly below.

First we only consider the radial variable integral which depicts near singularity in the Eq. (10), as follows:

$$I_1 = \int_{\rho_1(\theta)}^{\rho_2(\theta)} \frac{g(\rho,\theta)}{\rho^l} d\rho \tag{30}$$

Second we make a stretching transformation

$$\rho = \rho_1(\theta)\xi_1 \tag{31}$$

Eq. (31) becomes the following form:

$$I_1 = \int_{1}^{\frac{\rho_2(\theta)}{\rho_1(\theta)}} \frac{\rho_1(\theta) g(\xi_1,\theta)}{(\xi_1)^l} d\xi_1 \tag{32}$$

Then we make a logarithmic transformation to smooth out the rapid variations of the integrand

$$\xi_2 = \log(\xi_1) \tag{33}$$

Using Eq. (34), we have

$$I_1 = \int_{0}^{\log(\frac{\rho_2(\theta)}{\rho_1(\theta)})} \frac{\rho_1(\theta) e^{\xi_2} g(e^{\xi_2},\theta)}{(e^{\xi_2})^l} d\xi_2 \tag{34}$$

Finally, also adjusting the interval of integration within [-1, 1] for performing the standard Gaussian quadrature directly, the following transformation is given.

$$\xi_2 = k_1(\xi + 1) \tag{35}$$

where $k_1 = \frac{1}{2}\log(\frac{\rho_2(\theta)}{\rho_1(\theta)})$

Substituting Eq. (36) into Eq. (35), we have

$$I_1 = \int_{-1}^{1} \frac{k_1\rho_1(\theta)e^{k_1(\xi+1)}g(e^{k_1(\xi+1)},\theta)}{(e^{k_1(\xi+1)})^l}d\xi \tag{36}$$

We integrate all steps above and the final transformation is obtained as

$$\rho = \rho_1(\theta)e^{k_1(\xi+1)} \tag{37}$$

5.3 Case 3: $r_0 \neq 0$ and the projection point outside the element.

When $r_0 \neq 0$ and the projection point is outside the element, as shown in Fig. 3(c) and Fig. 4. When the source point is located on the side surface and the integration element is on the top surface, the projection point happens to be located outside the integration element. The process of constructing variable transformations is very similar to that described in Section 5.2. By applying the same steps as Section 5.2, a new transformation can be constructed.

$$\rho = r_0(e^{k_1\xi_4 + k_2} - 1) \tag{38}$$

where $k_1 = \frac{1}{2}\log(\frac{\rho_2(\theta)}{r_0} + 1) - \frac{1}{2}\log(\frac{\rho_1(\theta)}{r_0} + 1)$, $k_2 = \frac{1}{2}\log(\frac{\rho_2(\theta)}{r_0} + 1) + \frac{1}{2}\log(\frac{\rho_1(\theta)}{r_0} + 1)$

6. Element subdivision

The element subdivision is indispensible for treating the nearly singular integrals in the 3D cases as in Refs. [11, 27, 29]. In this section, we subdivide an integration element in a suitable pattern considering both element shape and the position of the projection point in the element. Adaptive integration based on element subdivision to calculate integrals is employed just as a combination for the new variable transformations [4]. The element subdivision technique is very similar to that discussed in Ref. [11], but more cases are considered.

Note that although the original quadrangle has a fine shape, the four subtriangles may have poor shapes depending on the position of $\mathbf{x}^c$ (the projection point) (see Fig. 6.(a)). Obtaining triangles of fine shape seems more difficult by direct subdivision for irregular initial elements as shown in Fig. 6(a) even $\mathbf{x}^c$ is located at the element center. If the angle denoted by θ, Fig. 6(b) – 6(f) between two lines in common with end point $\mathbf{x}^c$ in each triangle is larger by a certain value $2\pi/3$ and even tends to π, numerical results will become less accurate.

To solve the troubles described above, we have developed an adaptive subdivision for an arbitrary quadrilateral element. The original element is divided into several triangles and additional quadrangles, which is different from these as shown in Fig. 6 (a_1)-(f_1). The adaptive subdivision consists of three main steps described briefly as follows:

First, compute the distances in the real-world-coordinate system form $\mathbf{x}^c$ to each edge of the element and obtain the minimum distance d.

Then, based on d, we construct a box defined in parametric system, but with square shape in the real- world -coordinate system as can as possible, to well cover $\mathbf{x}^c$.

Finally, triangles are constructed from the box and additional quadrangles are created outside the box in the element.

Applying the strategy above, adaptive subdivisions for the elements in Fig. 6 with suitable patterns are shown in Fig. 6(a_1)-(f_1). For each triangle, the nearly singular integrals are calculated by the scheme discussed in Section 5. However, for each quadrangle, nearly singular integrals will arise but not severe, which can be calculated by adaptive integration scheme based on the element subdivision technique discussed in Refs. [8, 9]. It should be noted that, although the element subdivision is adopted, the computational cost is reduced dramatically compared with the conventional subdivision technique to compute nearly singular integrals on the whole element. This is because that the integrals on the local region of the element, which is more close to the source point, are calculated by the new variable transformations technique.

However, there is still another problem that how to combine new variable transformations with element subdivision technique when the projection point is located outside the integration element. Only a few literatures refer to nearly singular integrals of this type, such as the tangential transformation in Ref. [30]. In our implementation, when the projection point is located outside the integration element, the element subdivision technique is discussed as follows. As shown in Fig. 7(a), the element is subdivided into two triangles (region 1 and region 3) and a quadrangle (region 2) around the projection point. For the triangles and the quadrangle, transformation (37) or (46) is employed. However, the results obtained by this subdivision are not quite accurate. So, another subdivision is also employed in our method, as shown in Fig. 7(b). The point $\mathbf{x}^d$ which is the most close point to the source point in the element is introduced. We subdivide the element in three triangles around $\mathbf{x}^d$ instead of the projection point. And the transformations (29a) and (29b) are employed for nearly singular integrals in each triangle. The results obtained by this subdivision are very accurate. In Example 2, we compare the results of the two subdivisions and also try to find the causes.

7. Numerical examples

In this section, we will give a number of examples to investigate the effectiveness of different variable transformations. For the purpose of error estimation, the relative error is defined as follows:

$$error = \left| \frac{I_{nume} - I_{exact}}{I_{exact}} \right| \tag{39}$$

Where the subscripts *nume* and *exact* refer to numerical solutions and exact solutions respectively. In this paper, the exact solutions are obtained by adaptive element subdivisions techniques in Refs. [8, 9, 25, 26], and a large number of integration points are used. While in our method, we use 10×10 Gaussian points in all cases for the convenience of comparison.

Example 1:
$$\int_{-1}^{1}\int_{-1}^{1} \frac{\Phi_i(s,t)}{\sqrt{(s-s_0)^2+(t-t_0)^2+c^2}}\,dsdt \tag{40}$$

In first example, nearly singular integrals of Eq. (40) type [37] are considered. Where $\Phi_i(s,t)$ is a polynomial function, and s_0, $t_0 \in [-1,1]$, $c \in (0,1)$. $\Phi_i(s,t)$ is a quadratic basis function. For example, $\Phi_5(s,t) = (1-s^2)(1-t^2)$, $\Phi_9(s,t) = s(1+s)t(1+t)/4$. The relative errors listed in Table 1, compared with the *sinh* method [21, 22], *rad-ang* methods [37] and *Scuderi's* method [36].

Remark 1: From Table 1, it can be noted that when c>0.01, the sinh method produces superior results to our method. However, when c becomes smaller, the efficiency of the *sinh* method decreases, and the efficiency of our method and *Scuderi*'s *method* remains nearly constant. Compared with the *rad-ang* method and *Scuderi*'s *method*, in most cases, better results are obtained by our method. Moreover, the proposed method is effective in both coordinate systems.

Example 2: a regular planar rectangular boundary element

This example considers nearly singular integrals on a planar rectangular boundary element with the node coordinates of (0,0,0), (1,0,0), (1,1,0), (0,1,0). Relative errors of various integrals are listed in Table 2 and Table 3. In Table 2 and Table 3, $\mathbf{x}^c$ is the projection point and $\mathbf{x}^d$ is the most close point to the source point in the element.

Remark 2: From Table 2 and Table 3, it can be found that when the projection point is located outside the integration element, the element subdivision around the nearest point to the source point compared with the transformation (29a) and (29b) are effective. The relative errors are very small with the order less than 10^{-7} for integrals with kernel u^*. And for integrals with kernel $1/r^2$, the relative errors increase up to 10^{-5}. However, the element subdivision around the projection point compared with the transformation (37) or (38) is not so effective. The causes may be explained as follows:

1. The shapes of sub-triangles or sub-quadrangles are not quite fine, as shown in Fig. 7(a). The shape of the sub-quadrangle (region 2) in Fig. 7(a) is poor. In other words, in that sub-quadrangle, the bottom edge is very longer than the top edge.

2. As shown in Fig. 7(a), the polar coordinate transformation is used at the projection point $\mathbf{x}^c$. In the triangle (region 1), the lower and upper limits of the integral (Eq. (10)) $\rho_1 = d_1/\cos\theta$ and $\rho_2 = -d_4/\sin\theta$. In the quadrangle (region 2), they are $\rho_1 = d_1/\cos\theta$ and $\rho_2 = d_3/\cos\theta$. In the triangle (region 3), they are $\rho_1 = d_1/\cos\theta$ and $\rho_2 = d_2/\sin\theta$. The low limit becomes smaller when the projection point

approaches the element. The coefficient $k_1 = 0.5\log(\rho_2(\theta)/\rho_1(\theta))$ in transformation (37) may be very large, thus the results are affected.

3. The distributions of the integration points are shown in Fig. (8). In Fig. (8a), it can be seen that the inner integration points are crowded together around the projection point and the integration points of the top row are scattered and nearly overlap with each other . However, in Fig. (8b), the integration points concentrated around the nearest point are well arranged as in Fig. (8c), so better results can be obtained by the element subdivision around the nearest point using Eq. (29a) or Eq. (29b).

Example 3: an irregular planar rectangular boundary element

The second example considers nearly singular integrals on an irregular planar rectangular boundary element with the node coordinates of (0,0,0), (1,0,0) , (4,1,0), (0,4,0). The local coordinates of the projection point are set at (0.5, 0.5). Relative errors of various integrals are listed in Table 4. The symbol *NDivd* denotes the results obtained by the variable transformation only, while *Divd* denotes the results obtained by the variable transformation in combination with the element subdivisions.

Remark 3: From Table 4, it can be found that the new transformations technique in combination with element subdivisions is a very efficient scheme to calculate nearly singular integrals over an irregular quadrilateral boundary element. Compared with the conventional element subdivision techniques, the cost of computation is reduced dramatically, and a large number of integration points concentrated near the projection point are avoided. It also can be found that with the combined method the relative error of the results of various integrals is less than 10^{-5}, and that the results keep steady and accurate even the relative distance at 10^{-5}. And in most cases, we can get better results with the transformation (29b). The cause may be explained as follows: as shown in Fig. (9a) and (9b), the integration point is more concentrated near the projection point and integration points of the innermost layer nearly coincide with the projection point.

Example 4: a spherical surface element

This example considers nearly singular integrals on a curved surface element. The curved surface element is presented in parametric form by a local spherical polar system (θ,φ), and this kind element is named as spherical surface element here which is used in usually BFM [8, 9]. The element's geometric parameters are given as follows: $\theta \in [0,\pi/4]$, $\varphi \in [\pi/4,\pi/2]$ and the sphere radius (r) is set to 0.1, with

center $(0,0,0)$. The projection point of the given source point is located on the center of the element. In this example, we consider the high order shape function. The shape function is expressed as follows

$$\Phi = (t_1 + t_2 - 1)(1 + t_1)(1 + t_2)/4 \tag{41}$$

The *ratio* is the ratio of the distance between the source point and the projection point to the sphere radius. Various integrals are computed by Eq. (29a) and Eq. (29b) in two local systems. The relative errors are listed in Table 5.

Remark 4: Unlike the previous examples, the shape function is also considered in this special example. From Table 5, it can be found the transformation in two local systems is effective. The relative errors are very small with the order less than 10^{-5} for integrals with kernel u^*. And for integrals with kernel q^* and u_1^*, the relative errors increase up to 10^{-4}. The results denote that our method can be directly used for the curved surface element with high order shape functions in BEM.

7. Conclusions

Several new variable transformations are presented in this paper for accurate computation of nearly singular integrals arising in 3D BEM. It is an extension of the author's previous work [4] for 2D BEM.

The new variable transformations are based on the distance function which is constructed in two local systems described by (ρ,θ) and (α,β). In each local system, Taylor expansion is applied. Then the new transformations are derived for different cases in terms of the minimum distance and the positions of the projection point. These transformations are finally unified into a uniform formulation, which can deal with the integrals with near weak or strong singularity directly. For irregular elements, these new transformations combined with adaptive element subdivision considering both the element shape and the position of the projection point are applied to compute the nearly singular integrals. So, better results can be obtained. Moreover, the combined method reduces the cost of the convention element subdivision techniques. And the overall integration points are also reduced.

A number of numerical examples are presented on planar surface elements and curved surface elements. Results demonstrate that our method is accurate and effective.

1. For nearly hypersingular integrals, the present method is not so effective. Using the Ma's method [27, 29], it is easy to extend our method for nearly hypersingular integrals.

2. The accuracy of the present method is sensitive to the position of the projection point. However, as we know, it is difficult to find the ideal projection point in many cases, so how to reduce the sensitiveness on the position of the projection point is important for us to perform the method.

Works on these problems are undergoing and we will report them in following papers.

ACKNOWLEDGEMENT

This work was supported in part by National Science Foundation of China under grant numbers 11172098, in part by national project under grant number 2011ZX04003-011, in part by National 973 Project of China under grant number 2010CB328005 and in part by Hunan Provincial Natural Science Foundation for Creative Research Groups of China (Grant No.12JJ7001).

REFERENCES

1. Cruse TA, Aithal R. Non-singular boundary integral equation implementation. International Journal for Numerical Methods in Engineering 36 (1993) 237–254.
2. Liu YJ. Analysis of shell-like structures by the boundary element method based on 3-D elasticity: Formulation and Verification. International Journal for Numerical Methods in Engineering 41 (1998) 541–558.
3. Krishnasamy G, Rizzo FJ, Liu YJ. Boundary integral equations for thin bodies. International Journal for Numerical Methods in Engineering 37 (1994) 107–121.
4. G.Z. Xie, J.M. Zhang, X.Y. Qin, G.Y. Li, New variable transformations for evaluating nearly singular integrals in 2D boundary element method, Engineering Analysis with Boundary Elements 35 (2011) 811-817.
5. Dirgantara T, Aliabadi MH. Crack growth analysis of plates loaded by bending and tension using dual boundary element method. International journal of fracture 105 (2000) 27–47.
6. Aliabadi MH, Martin D. Boundary element hypersingular formulation for elasto-plastic contact problems. International Journal for Numerical Methods in Engineering 48 (2000) 995–1014.
7. Zhang D, Rizzo FJ, Rudolphi TJ. Stress intensity sensitivities via hypersingular boundary integral equations. Computational mechanics 23 (1999) 389–396.
8. Zhang JM, Qin XY, Han X, Li GY. A boundary face method for potential problems in three dimensions. International Journal for Numerical Methods in Engineering 80 (2009) 320–337.
9. Qin XY, Zhang JM, Li GY, et al. An element implementation of the boundary face method for 3D potential problems. Engineering Analysis with Boundary Elements 34 (2010) 934-943
10. F.L. Zhou, J.M. Zhang, X.M. Sheng, G.Y. Li, Shape variable radial basis function and its application in dual reciprocity boundary face method, Engineering Analysis with Boundary

Element 35 (2011) 244-252.

11. X.Y. Qin, J.M. Zhang, G.Z. Xie, F.L. Zhou, A general algorithm for the numerical evaluation of nearly singular integrals on 3D boundary element, Journal of computational and applied mathematics 235 (2011) 4174-4186
12. F.L. Zhou, J.M. Zhang, X.M. Sheng, G.Y. Li, A dual reciprocity boundary face method for 3D non-homogeneous elasticity problems, Engineering Analysis with Boundary Elements 36 (2012) 1301-1310.
13. F.L. Zhou, G.Z. Xie, J.M. Zhang, X.S. Zheng, Transient heat conduction analysis of solids with small open-ended tubular cavities by boundary face method, Engineering Analysis with Boundary Elements 37 (2013) 542-550.
14. Chen HB, Lu P, Huang MG, Williams FW. An effective method for finding values on and near boundaries in the elastic BEM. Computers & structures 69 (1998) 421–431.
15. Sladek N, Sladek J, Tanaka M. Regularization of hypersingular and nearly singular integrals in the potential theory and elasticity. International Journal for Numerical Methods in Engineering 36 (1993) 1609–1628.
16. Liu YJ, Rudolphi TJ. New identities for fundamental solutions and their applications to non-singular boundary element formulations. Computational mechanics 24 (1999) 286–292.
17. Liu YJ. On the simple solution and non-singular nature of the BIE/BEM–a review and some new results. Engineering Analysis with Boundary Element 24 (2000) 789–795.
18. Krishnasamy G, Schmerr LW, Rudolphi TJ, Rizzo FJ. Hypersingular boundary integral equations: some applications in acoustic and elastic wave scattering. Journal of Applied Mechanics (57) 1990 404–414.
19. Niu ZR, Wendland Wl, Wang XX, Zhou HL. A sim-analytic algorithm for the evaluation of the nearly singular integrals in three-dimensional boundary element methods. Computer methods on applied mechanics and engineering 31 (2005) 949–64.
20. Zhou HL, Niu ZR, Cheng CZ, Guan ZW. Analytical integral algorithm applied to boundary layer effect and thin body effect in BEM for anisotropic potential problems. Computers & structures 86(2008) 1656-1671.
21. Peter R. Johnston, David Elliott. A sinh transformation for evaluating nearly singular boundary element integrals. International Journal for Numerical Methods in Engineering 62 (2005) 564-578.
22. Barbara M. Johnston, Peter R. Johnston, David Elliott. A sinh transformation for evaluating two-dimensional nearly singular boundary element integrals. International Journal for Numerical Methods in Engineering 69(2007) 1460-1479.
23. David Elliott, Peter R. Johnston .Error analysis for a sinh transformation used in evaluating nearly singular boundary element integrals. Journal of computational and applied mathematics 203 (2007) 103-124.
24. Tells,J.C.F. A self adaptive coordinate transformation for efficient numerical evaluations of

general boundary element integrals, International Journal for Numerical Methods in Engineering 24 (1987) 959-973.

25. Gao XW, Davies TG. Adaptive integration in elasto-plastic boundary element analysis. Journal of the Chinese institute of engineers 23 (2000) 349-356.
26. J.C. Lachat, J.O. Waston, Effective numerical treatment of boundary integral equations: a formulation for three-dimensional elastostatics, International Journal for Numerical Methods in Engineering 10 (1976) 273–289.
27. Ma H, Kamiya N. A general algorithm for the numerical evaluation of nearly singular boundary integrals of various orders for two- and three-dimensional elasticity. Computational mechanics 29 (2002) 277-288.
28. Ma H, Kamiya N. A general algorithm for accurate computation of field variables and its derivatives near boundary in BEM. Engineering Analysis with Boundary Elements 25 (2001) 833–841.
29. Ma H, Kamiya N. Distance transformation for the numerical evaluation of near singular boundary integrals with various kernels in boundary element method. Engineering Analysis with Boundary Elements 26 (2002) 329-339.
30. Ma H, Kamiya N. Nearly singular approximations of CPV integrals with end and corner-singularities for the numerical solution of hypersingular boundary integral equations. Engineering Analysis with Boundary Elements 27 (2003) 625-637.
31. Hayami, K. and Matsumoto, H. A numerical quadrature for nearly singular boundary element integrals. Engineering Analysis with Boundary Elements 13 (1994) 143-154.
32. Hayami, K., Variable transformations for nearly singular integrals in the boundary element method. Publications of Research Institute for Mathematical Sciences, Kyoto University, 41 (2005) 821-842.
33. K. Hayami, C.A. Brebbia, Quadrature methods for singular and nearly singular integrals in 3-D boundary element method, in: C.A. Brebbia (Ed.), Boundary Elements X, Spring-Verlag, 1988, pp. 237-264
34. Zhang YM, Gu Y, Chen JT. Boundary layer effect in BEM with high order geometry elements using transformation. Computer Modeling in Engineering and Sciences 45 (2009) 227-247.
35. Zhang YM, Gu Y, Chen JT. Boundary element analysis of the thermal behaviour in thin-coated cutting tools. Engineering analysis with boundary elements 34 (2010) 775-784.
36. Scuderi, Letizia. "On the computation of nearly singular integrals in 3D BEM collocation." International journal for numerical methods in engineering 74.11 (2008): 1733-1770.
37. Hayami K, Brebbia CA. A new coordinate transformation method for singular and nearly singular integrals over general curved boundary elements. In Boundary Elements IX , Proceedings of the 9th International Conference on Boundary Elements, Stuttgart, Brebbia CA, Wendland WL, Kuhn G (eds), vol. 1. A Computational Mechanics Publications with Springer-Verlag: Berlin, 1987; 375–399.

Fig.1. The minimum distance r_0, from the source point **y** to the 3D curved surface element

Fig. 2. Nearly singular integration on an element (*a*) A quadrilateral element in local parametric system (t_1, t_2) when the projection point is in the element (*b*) Subdivisions of the quadrilateral element (*c*) A triangle is mapped into a square in (α, β) coordinate system

Fig. 3. Three cases considering r_0 and the position of $\mathbf{x}^c$ (a) $r_0 \neq 0$ and $\mathbf{x}^c$ is in the element (b) $r_0 = 0$ and the projection point is outside the element (c) $r_0 \neq 0$ and $\mathbf{x}^c$ is outside the element

Fig .4. A thin plate.

Fig. 5. Two types of the element: (a) Discontinuous elements (b) Element sizes quite are different

Fig. 6. Subdivisions of quadrilateral element depending on the position of the projection point $\mathbf{x}^c$

Fig. 7. Subdivisions of quadrilateral element when the projection point outside the integration element

Fig. 8. Distributions of the integration points

(a) The integration points of the element subdivision around the projection point using Eq. (37) (The number is 300).

(b) The integration points of the element subdivision around the nearest point using Eq. (29a) (The number is 300).

(c) The integration points when the projection point is in the center of the element (The number is 400).

Fig. 9. Distributions of the integration points of three methods

(a) The integration points of transformation (29a) combined with the element subdivision (The number is 688).

(b) The integration points of transformation (29b) combined with the element subdivision (The number is 688).

(c) The integration points of adaptive element subdivision (The number is 2200).

Table 1 Relative errors of our method using Eq. (29a) and Eq. (29b) compared with the other methods

Table 2 Relative errors of various integrals when $r_0 = 0$

Table 3 Relative errors of various integrals when $r_0 \neq 0$

Table 4 Relative errors of various integrals using Eq. (29a) and Eq. (29b) in combination with element subdivisions.

Table 5 Relative errors of various integrals on the spherical surface element with Eq. (29a) and Eq. (29b).

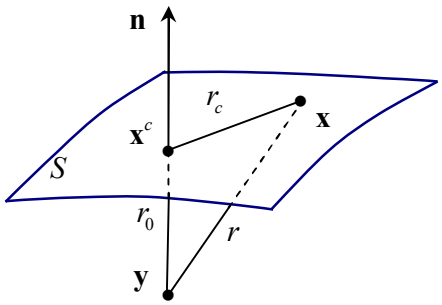

Fig.1. The minimum distance r_0, from the source point **y** to the 3D curved surface element

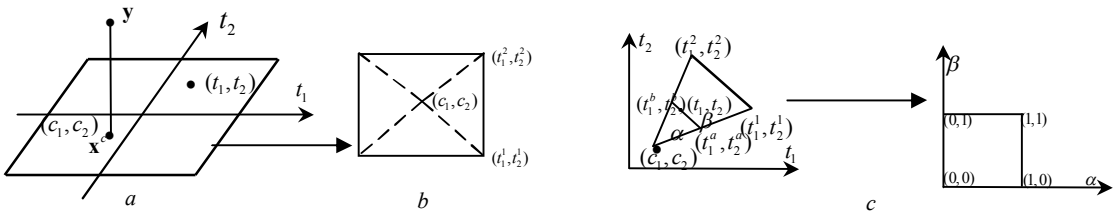

Fig. 2. Nearly singular integration on an element (*a*) A quadrilateral element in local parametric system (t_1, t_2) when the projection point is in the element (*b*) Subdivisions of the quadrilateral element (*c*) A triangle is mapped into a square in (α, β) coordinate system

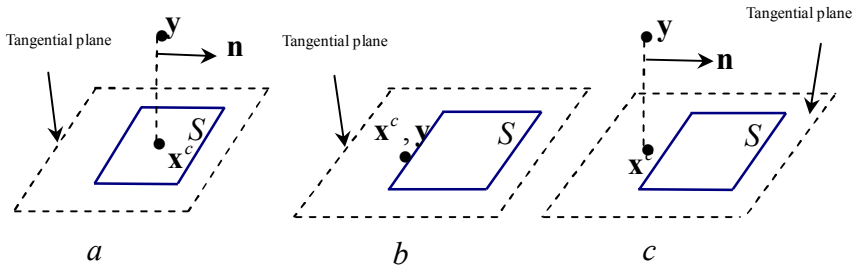

Fig. 3. Three cases considering r_0 and the position of $\mathbf{x}^c$ (a) $r_0 \neq 0$ and $\mathbf{x}^c$ is in the element (b) $r_0 = 0$ and the projection point is outside the element (c) $r_0 \neq 0$ and $\mathbf{x}^c$ is outside the element

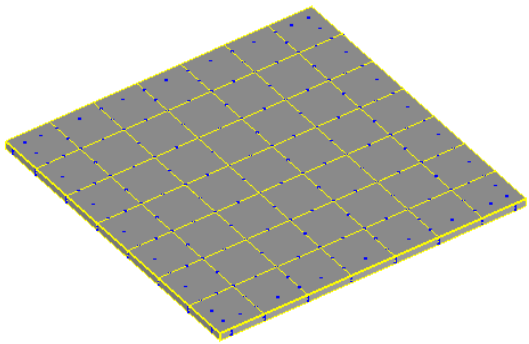

Fig .4. A thin plate.

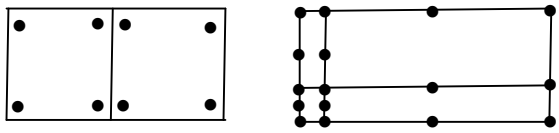

Fig. 5. Two types of the element: (a) Discontinuous elements (b) Element sizes quite are different

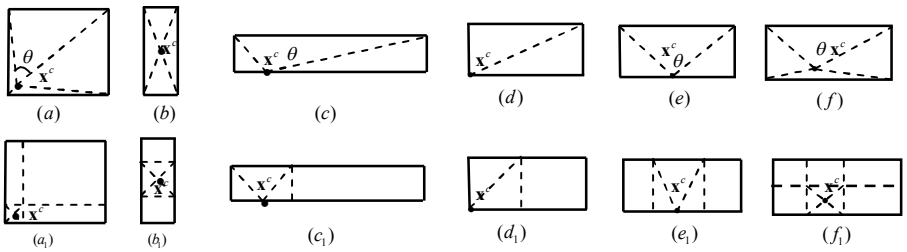

Fig. 6. Subdivisions of quadrilateral element depending on the position of the projection point

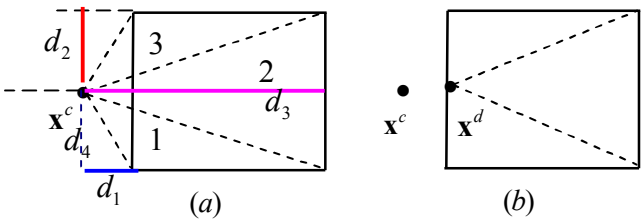

Fig. 7. Subdivisions of quadrilateral element when the projection point outside the integration element

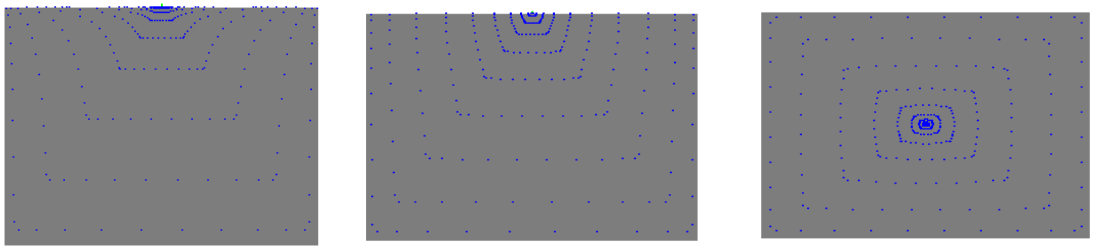

Fig. 8. Distributions of the integration points

(a) The integration points of the element subdivision around the projection point using Eq. (37) (The number is 300).

(b) The integration points of the element subdivision around the nearest point using Eq. (29a) (The number is 300).

(c) The integration points when the projection point is in the center of the element (The number is 400).

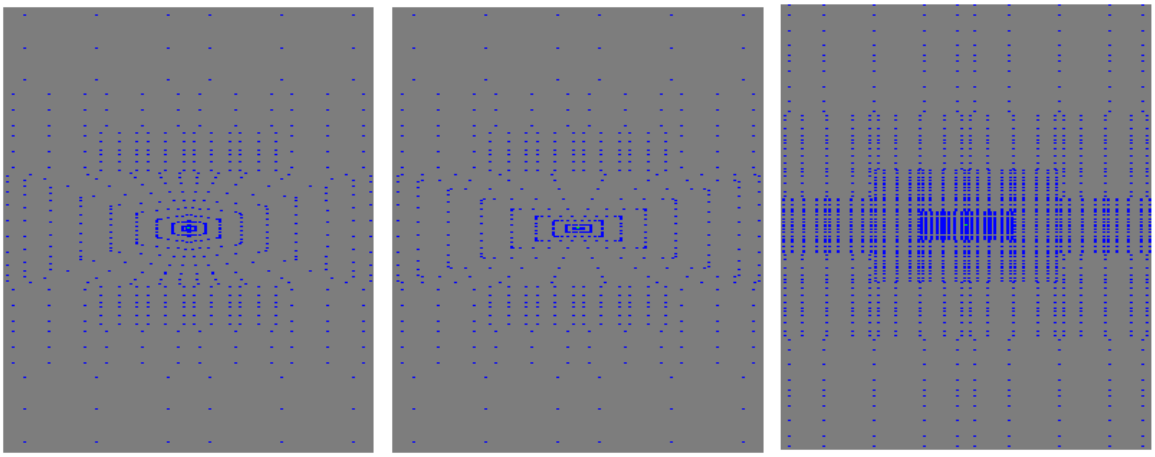

a *b* *c*

Fig. 9. Distributions of the integration points of three methods

(a) The integration points of transformation (29a) combined with the element subdivision (The number is 688).

(b) The integration points of transformation (29b) combined with the element subdivision (The number is 688).

(c) The integration points of adaptive element subdivision (The number is 2200).

	$\Phi_5(s,t)$, s_0=0.5, t_0=0.5			
	c=0.1	c=0.01	c=0.001	c=0.0001
Scuderi's *method*	1.16E-07	1.14E-07	3.68E-07	1.08E-07
rad-ang	4.57E-05	8.40E-06	2.87E-07	3.51E-09
sinh	1.02E-11	4.37E-08	4.77E-06	2.72E-05
(α,β)	1.46E-09	3.64E-09	3.67E-09	8.41E-09
(ρ,θ)	9.32E-11	1.22E-09	6.80E-09	1.65E-08
	$\Phi_5(s,t)$ s_0=0.0, t_0=0.9			
	c=0.1	c=0.01	c=0.001	c=0.0001
Scuderi's *method*	1.08E-07	1.00E-07	9.38E-08	1.14E-07
rad-ang	1.27E-04	2.62E-05	1.24E-06	2.08E-08
sinh	2.10E-12	1.76E-08	1.44E-06	4.44E-06
(α,β)	8.94E-11	3.09E-10	5.78E-10	6.75E-10
(ρ,θ)	8.94E-11	7.19E-11	1.50E-09	2.34E-09
	$\Phi_9(s,t)$ s_0=0.9, t_0=0.9			
	c=0.1	c=0.01	c=0.001	c=0.0001
Scuderi's *method*	8.59E-07	3.59E-07	1.20E-07	6.04E-07
rad-ang	4.89E-04	6.70E-05	2.88E-06	4.38E-08
sinh	1.75E-13	5.54E-08	6.64E-06	4.56E-05
(α,β)	1.47E-11	2.27E-09	3.90E-09	4.01E-09
(ρ,θ)	1.42E-10	1.93E-10	1.29E-08	2.18E-08

Table 1 Relative errors of our method using Eq. (29a) and Eq. (29b) compared with the other methods

	integrals with kernel u^*, source point (0.5, -c, *0*), $\mathbf{x}^c$=(0.5, -c)				
	c=0.1	c=0.01	c=0.001	c=0.0001	c=0.00001
Exact solution	0.14617613077	0.18330947792	0.19028609486	0.19131325733	0.19144895251
Eq. (37)	5.70E-09	1.70E-04	6.79E-04	2.32E-04	4.21E-04
	integrals with kernel u*, source point (0.5, -c, 0), $\mathbf{x}^d$=(0.5, 0)				
Eq.(29a)	7.27E-12	9.85E-09	1.64E-08	1.19E-08	1.73E-09
Eq.(29b)	3.05E-10	1.13E-08	6.94E-09	1.17E-08	8.02E-10
	integrals with kernel $1/r^2$, source point (0.5, -c, 0), $\mathbf{x}^c$=(0.5, -c)				
	c=0.1	c=0.01	c=0.001	c=0.0001	c=0.00001
Exact solution	4.56481792601	11.3647236099	18.5542488609	25.7835995636	33.0169405280
Eq. (37)	5.57E-10	2.95E-05	3.29E-04	4.34E-04	3.79E-04
	integrals with kernel u^*, source point (0.5, -c, *0*), $\mathbf{x}^d$=(0.5, 0)				
Eq.(29a)	2.22E-09	1.37E-06	1.37e-05	1.29E-06	7.27E-05
Eq.(29b)	4.29E-09	1.62E-07	6.60E-06	9.45E-06	9.39E-05

Table 2 Relative errors of various integrals when r_0=0

	integrals with kernel u^*, source point $(0.5, -c, c)$, $\mathbf{x}^c=(0.5, -c)$				
	c=0.1	c=0.01	c=0.001	c=0.0001	c=0.00001
Exact solution	0.1407740622	0.1826286656	0.1902164314	0.1913062749	0.1914482540
Eq. (38)	6.01E-09	1.71E-04	6.80E-04	2.32E-04	4.21E-05
	integrals with kernel u^*, source point $(0.5, -c, c)$, $\mathbf{x}^d=(0.5, 0)$				
Eq.(29a)	2.05E-11	1.91E-09	1.08E-08	2.40E-08	2.13E-09
Eq.(29b)	8.16E-11	1.74E-08	2.10E-08	1.89E-08	7.48E-10
	integrals with kernel $1/r^2$, source point $(0.5, -c, c)$, $\mathbf{x}^c=(0.5, -c)$				
	c=0.1	c=0.01	c=0.001	c=0.0001	c=0.00001
Exact solution	4.0016235178	10.773731294	17.962921594	25.192268883	32.425609808
Eq. (38)	1.37E-09	3.11E-05	3.40E-04	4.41E-04	3.73E-04
	integrals with kernel $1/r^2$, source point $(0.5, -c, c)$, $\mathbf{x}^d=(0.5, 0)$				
Eq.(29a)	1.81E-10	6.79E-07	1.35E-05	8.67E-06	1.23E-04
Eq.(29b)	1.30E-09	4.89E-07	3.37E-06	1.87E-05	7.40E-05

Table 3 Relative errors of various integrals when $r_0 \neq 0$

		integrals with kernel u^*, source point (0.5, 2, c), $\mathbf{x}^c$=(0.5, 0.5)				
		c=0.2	c=0.02	c=0.002	c=0.0002	c=0.00002
Exact solution		0.403729220	0.481057107	0.489927211	0.490825911	0.4909158987
(ρ,θ)	*NDivd*	8.76E-05	3.28E-04	3.64E-04	3.68E-04	3.68E-04
	Divd	8.05E-06	6.34E-06	6.21E-06	6.17E-06	6.18E-06
(α,β)	*NDivd*	6.05E-04	1.80E-03	1.90E-03	1.90E-03	1.90E-03
	Divd	4.95E-10	3.12E-09	4.04E-09	3.01E-10	4.60E-09
		integrals with kernel q^*, source point (0.5, 2, c), $\mathbf{x}^c$=(0.5, 0.5)				
		c=0.2	c=0.02	c=0.002	c=0.0002	c=0.00002
Exact solution		0.374991104	0.486882560	0.498687581	0.499868757	0.4999868757
(ρ,θ)	*NDivd*	9.04E-04	2.30E-03	2.10E-03	2.40E-03	4.44E-03
	Divd	3.25E-06	2.54E-06	1.62E-05	3.67E-04	6.43E-04
(α,β)	*NDivd*	5.10E-03	1.04E-02	1.09E-02	1.08E-02	1.02E-02
	Divd	6.06E-09	1.86E-08	2.44E-06	4.44E-05	1.56E-06

Table 4 Relative errors of various integrals using Eq. (29a) and Eq. (29b) in combination with element subdivisions.

integrals with kernel u^* and shape function, $\mathbf{x}^c=(0.5, 0.5)$					
ratio	10^{-1}	10^{-2}	10^{-3}	10^{-4}	10^{-5}
Exact solution	0.0021255434	0.002915264	0.0030119822	0.0030218499	0.0030228387
(ρ,θ)	5.47E-10	3.38E-10	3.32E-08	2.65E-07	1.92E-06
(α,β)	3.43E-10	3.43E-08	3.32E-08	4.30E-07	2.71E-06
integrals with kernel q^* and shape function, $\mathbf{x}^c=(0.5, 0.5)$					
ratio	10^{-1}	10^{-2}	10^{-3}	10^{-4}	10^{-5}
Exact solution	0.0857906725	0.133600754	0.1394520195	0.1400483568	0.1401081030
(ρ,θ)	7.77E-10	3.29E-08	5.75E-06	1.20E-04	6.96E-04
(α,β)	2.56E-08	7.26E-08	4.79E-06	2.73E-06	1.26E-04
integrals with kernel u_i^* and shape function, $\mathbf{x}^c=(0.5, 0.5)$					
ratio	10^{-1}	10^{-2}	10^{-3}	10^{-4}	10^{-5}
Exact solution	0.163903665	0.2145864699	0.2200517795	0.2206016447	0.220656664
(ρ,θ)	7.58E-11	3.63E-08	6.22E-06	1.82E-04	9.19E-04
(α,β)	2.47E-08	8.97E-08	5.19E-06	1.97E-04	7.55E-04

Table 5 Relative errors of various integrals on the spherical surface element with Eq. (29a) and Eq. (29b).